Article

Investigation of Laser Induced Graphene (LIG) on a Flexible Substrate and its Functionalization by Metal Doping for Gas-Sensing Applications

Dongwook Kwak , Hyojin Kim , Seung Hun Jang , Byoung Gak Kim , Donghwi Cho , Hyunju Chang , Jeong-O Lee *

Posted Date: 5 January 2024

doi: 10.20944/preprints202401.0424.v1

Keywords: Laser Induced Graphene (LIG); metal-doped graphene; flexible gas sensor; graphene surface functionalization; gas sensing mechanism of graphene

Article

Investigation of Laser Induced Graphene (LIG) on a Flexible Substrate and its Functionalization by Metal Doping for Gas-Sensing Applications

Dongwook Kwak [1], Hyojin Kim [1], Seung Hun Jang [2], Byoung Gak Kim [1], Donghwi Cho [1], Hyunju Chang [2] and Jeong-O Lee [1,*]

[1] Advanced Materials Division, Korea Research Institute of Chemical Technology, 141 Gajeongro, Yuseong-gu, Daejeon 34114, Republic of Korea
[2] Data Research Center, Korea Research Institute of Chemical Technology, 141 Gajeongro, Yuseong-gu, Daejeon 34114, Republic of Korea
* Correspondence: jolee@krict.re.kr; Tel.: +82-42-860-7336; Fax: +82-42-860-7508

Abstract: Graphene materials synthesized using direct laser writing (laser-induced graphene; LIG) are favorable sensor materials because of their large surface area, ease of fabrication, and cost effectiveness. In particular, LIG decorated with metal nanoparticles (NPs) has been used in various sensors, including chemical sensors and electronic and electrochemical biosensors. However, the effect of metal decoration on LIG sensors remains controversial; hypotheses based on computational simulations do not always match experimental results, and even experimental results reported by different researchers have not been consistent. In the present study, we explored the effects of metal decorations on LIG gas sensors, with NO_2 and NH_3 gases as representative oxidizing and reducing agents, respectively. To eliminate unwanted side effects arising from metal salt residues, metal NPs were directly deposited by vacuum evaporation. Although the gas sensitivities of the sensors deteriorate upon metal decoration irrespective of the metal work function in the case of NO_2 gas, they improve upon metal decoration in the case of NH_3 exposure. A careful investigation of the chemical structure and morphology of the metal NPs in the LIG sensors shows that the spontaneous oxidation of metal NPs with a low work function changes the behavior of the LIG gas sensors and that the sensor behaviors under NO_2 and NH_3 gases follow different principles.

Keywords: laser induced graphene (LIG); metal-doped graphene; flexible gas sensor; graphene surface functionalization; gas sensing mechanism of graphene

1. Introduction

The outstanding features of graphene, which include good thermal and chemical stability, high carrier mobility (~15 000 cm2·V−1·s−1), low electrical noise, and a high specific surface area (~2630 m2·g−1), have caused it to be actively studied and employed in a wide range of applications.[1–4] Graphene is composed of a single atomic layer of sp2-hybridized carbon atoms packed in a honeycomb crystal lattice in which the carbon–carbon bond length is 1.42 Å. This two-dimensional crystal nature makes graphene an attractive gas-sensing medium, with graphene offering the largest gas-adsorption area per unit volume among report gas-sensing media.[5] However, graphene suffers an inherent lack of selectivity and sluggish gas adsorption and desorption, resulting in slow response and recovery characteristics.[6] Consequently, extensive efforts have been devoted to enhancing the sensing performance of graphene-based gas detectors. To this end, several strategies have been proposed and investigated, including (1) functionalizing graphene with polymers, metal oxides, and noble metals, (2) engineering three-dimensional (3D) graphene nanostructures, and (3) optimizing sensor device configurations.[7] Among these strategies, metal doping into graphene is a well-known, simple, and efficient approach because of graphene's Dirac-cone band structure with a zero bandgap, which facilitates the facile modification of its Fermi level by external factors such as doping, leading to improvements of its gas-sensing characteristics.[3,8,9] Numerous first-principles studies based on density functional theory (DFT) have been conducted through measurements of the

 doi:10.20944/preprints202401.0424.v1

adsorption energy, bandgap, density of states (DOS), atom–carbon distance, and charge transfer characteristics, among other properties, to reveal how the relationship among metal dopants, graphene, and gaseous analytes affects the sensing response;[10–17]; however, the calculations were performed using ideal hypothetical models and not all experimental results can be successfully interpreted with the model system. Cho et al.[7,18] and Zhao et al. found that their experimental results sometimes differ from theoretical results reported in the literature. They also emphasized that the response process of the metal-doped graphene toward gas exposure is not straightforward; it is complicated by the interactions between metal dopants and graphene, graphene and gas molecules, and even metal dopants and gas molecules. Moreover, few practical and experimental studies on gas detection using metal-doped graphene have been reported, especially for graphene with 3D structures and defects, to support theoretical studies. To develop a high-performance graphene-based gas sensor with metal-doped graphene, clarifying the sensing mechanisms through correlated theoretical and experimental studies is strongly advised.

Compared with conventional techniques for the synthesis of graphene (e.g., chemical vapor deposition (CVD); micromechanical, electrochemical, and chemical exfoliation of graphite; and epitaxial growth), the laser direct writing (LDW) method provides distinct benefits such as low-cost manufacturing, rapid production, precision patterning capability, and the ability to fabricate graphene under ambient conditions, even though the obtained graphene is multilayered and contains a certain concentration of defects.[2,19,20] In addition, the LDW route is not only a scalable and effective method to manufacture 3D graphene with a structure more favorable for gas-sensing applications than the structure of 2D graphene but also enables functionalization of the graphene surfaces. Both top-down and bottom-up syntheses of 2D graphene involve high temperatures or harsh chemicals, and the irregular stacking of materials hinders the functionalization of surfaces.[21] An exceptional advantage of LDW over traditional methods is that it enables different physical properties (e.g., superhydrophilicity or superhydrophobicity) and various microstructures (e.g., sheet, foam, fiber, and nanodiamond formation) to be obtained by simply manipulating atmospheric conditions and controlling lasing parameters, respectively.[22] To realize such benefits, laser-induced graphene (LIG) has been actively investigated and used in sensor applications such as biosensors, humidity sensors, strain sensors, temperature sensors, piezo-resistive sensors, wearable body-condition sensors, and gas sensors.[1,2,23] In general, LIG can be formed on various substrate materials (e.g., polyetherimide (PEI), poly(ether ether ketone), polyethersulfone, polyimide (PI), polysulfone, paper, wood, and potato); however, in the case of gas-sensing applications, PI has been most frequently selected because of its good radiation resistance, low noise generation, exceptional thermal stability, and good endurance in harsh environments.[24,25]

In this article, we experimentally demonstrate and assess the gas-sensing responses of LIG-based gas sensor devices synthesized on a flexible PI substrate toward NO2 and NH3, which are representative oxidizing and reducing agents, respectively. Also, their sensing mechanisms and the influence of various metal dopants (Ag, Al, Au, Cu, In, and Pd) on the sensor response to the gaseous analytes are elucidated. Because our LIG exhibits p-type semiconducting behavior, both our pristine LIG (P-LIG) and metal-doped LIG (M-LIG) sensor devices exhibit negative responses (decreasing resistance) to an oxidizing agent (NO2) and positive responses (increasing resistance) to a reducing agent (NH3); however, the interactions among each type of metal nanoparticle (NP), LIG, and gas molecule alters the devices' electronic properties, which determines whether their sensing performance is enhanced or deteriorated. This work might provide guidance in selecting an appropriate metal dopant for 3D-structured graphene with a certain degree of defects in specific gas detection, enabling the development of a flexible and high-performance LIG gas sensor.

 doi:10.20944/preprints202401.0424.v1

2. Results and Discussion

2.1. Fabrication and Characterization of the P-LIG sensor device.

Figure 1a shows the P-LIG sensor with a serpentine pattern in the middle and two circles on the top and bottom (used for the Ag-pasted contact areas) synthesized on a flexible PI substrate. Upon irradiation of the substrate with a 10.6 μm CO_2 laser under ambient conditions, a pattern with a width of ~400 μm and thickness of ~22 μm and a circle with a 500 μm radius and thickness of ~22 μm were well formed on the 125 μm-thick PI film (Figure 1b and Figure S2b). Figure 1c confirms that the synthesized LIG had a highly porous structure, which is beneficial for gas adsorption because of its remarkably high specific surface area.

The Raman spectrum in Figure 1d shows the three typical peaks of graphene: the D peak (~1350 cm^{-1}), G peak (~1583 cm^{-1}), and the 2D peak (~2695 cm^{-1}). In general, the D peak is related to the breathing mode of sp^2 carbon in an aromatic formation, representing the existence of defects and disorder in graphene and serving as an indirect measure of the graphene quality. The G and 2D bands correspond to the in-plane vibration mode of sp^2-hybridized carbon networks and the stacking order of graphene along its *c*-axis, respectively. Because the I_{2D}/I_G and I_D/I_G values obtained from the Raman spectrum are to ~0.69 and ~0.79, the synthesized P-LIG is implied to have multilayer structure with a relatively low defect density.[26] In addition, on the basis of the Tuinstra–Koenig relation, the crystalline size of the P-LIG along the α-axis (L_a) was calculated to be ~389.36 nm using equation (1):[27]

$$L_a = (2.4 \times 10^{-10}) \times \lambda_l^4 \times \left(\frac{I_G}{I_D}\right) \quad (1)$$

where λ_l is the wavelength of the Raman laser (λ_l = 1064 nm).

The full-survey XPS spectrum in Figure 1e clearly shows that only the C1s (282.3 eV) and O1s (530.7 eV) peaks are detected in the spectrum of P-LIG and that their calculated atomic percentages are 94.9% and 5.1%, respectively, confirming the successful synthesis of LIG.

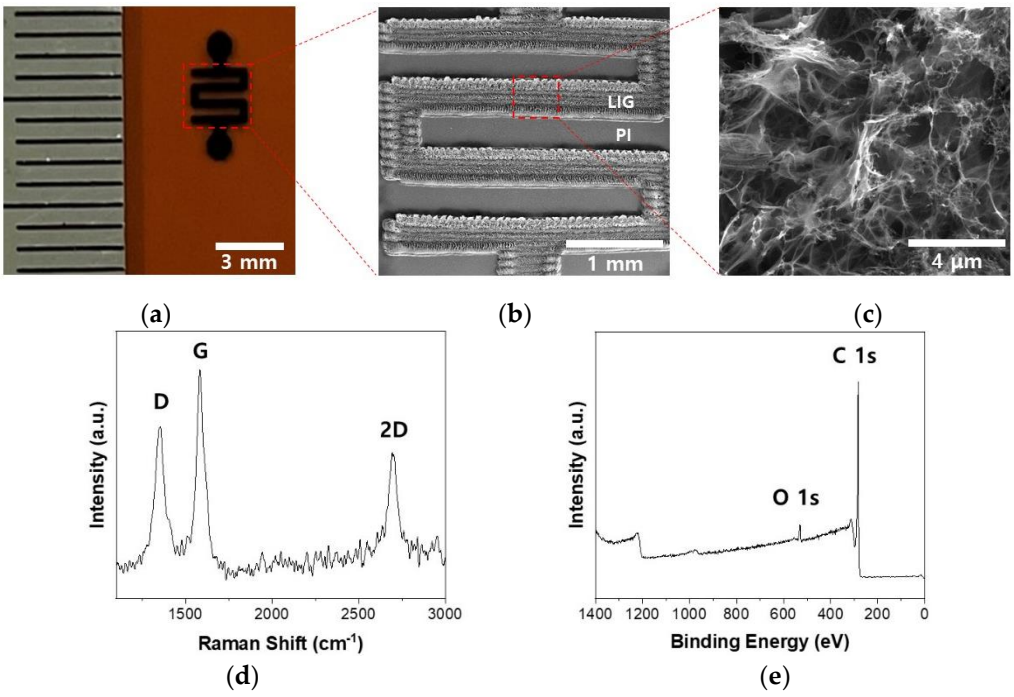

Figure 1. (a) Optical image of a P-LIG gas sensor on a PI film. (b,c) SEM image of the serpentine area with a ~400 μm-thick width. (d,e) Raman spectrum and XPS survey spectrum, respectively, of the P-LIG.

 doi:10.20944/preprints202401.0424.v1

2.2. Metal-doping in P-LIG and characterization of the M-LIG sensor devices

In the present study, the vacuum-evaporation method was used to functionalize LIG devices with metal NPs because the generally used method of heteroatom doping by direct writing in salt baths can result in unwanted residues.[28] As shown in Figure 2a, a metal stencil mask made of SUS304 was used to deposit metal NPs onto the pre-fabricated P-LIG sensor device and a total of 18 sensor devices were produced through a single deposition via thermal evaporation. A metal thickness of 4 nm was used in the fabrication of all of the M-LIG sensors because the formation of metal NPs was apparent when the metal deposition thickness was 4 nm (as measured using a QCM), as shown in Figure S2f. A computer-based design tool (AutoCAD and CorelDRAW) enabled fine alignment between the stencil mask and the P-LIG sensor devices; EDS mapping images presented in Figure 2b and Figure S2d reveal that the deposited metal NPs were well-dispersed on the targeted serpentine area and on the surface of the LIG. To observe the interaction between the metal dopants and LIG, we carried out XPS analysis. Compared with the surface of the P-LIG, the surfaces of all of the M-LIGs exhibited substantial metal oxidation (Figure 2c). In addition, the high-resolution survey (Figure S3) and quantification results (Table S1) reveal that greater oxidation occurred in the Al-, Cu-, and Pd-doped LIG devices than in the devices doped with other metals. Notably, the readily oxidized AlO_x shell–Al NPs can be formed on the surface of graphene because the Al metal has a high oxidation rate; thus, the Al-doped LIG sensor device exhibited the highest degree of oxidation among the investigated devices.[29]

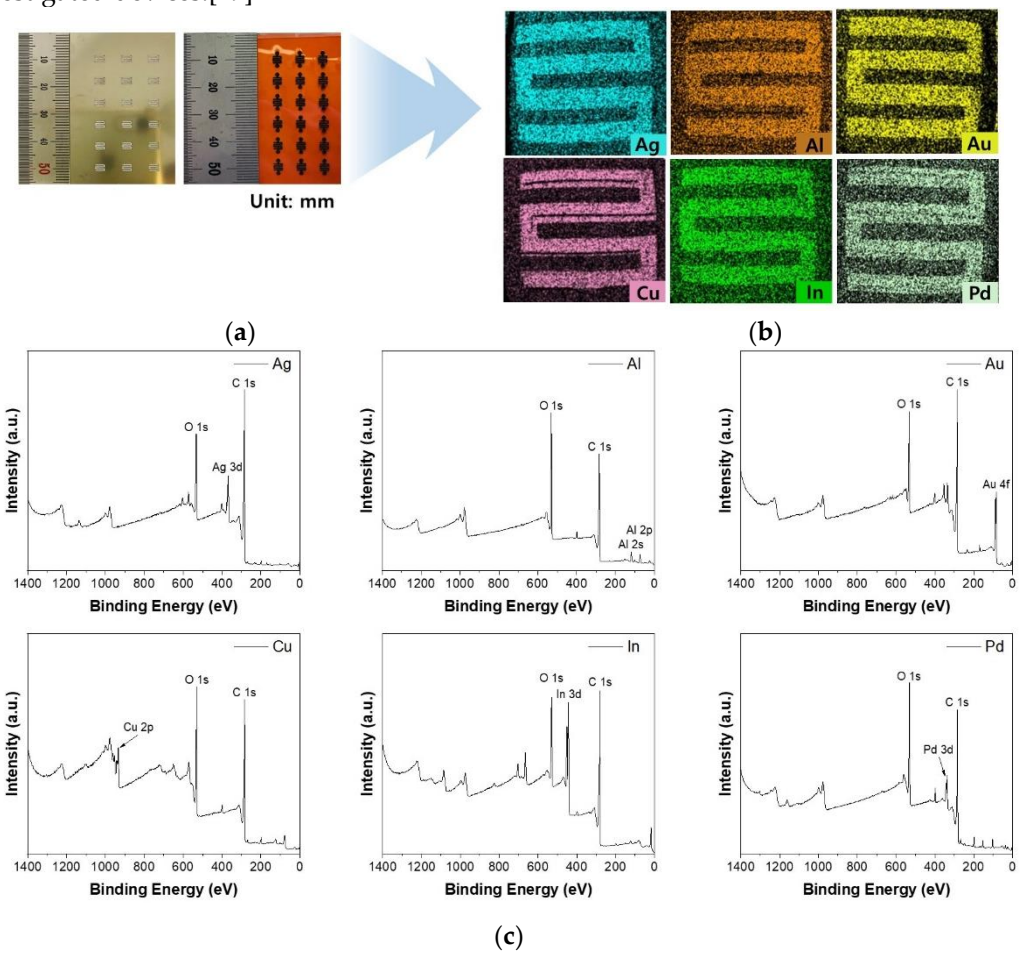

Figure 2. (a) Metal stencil mask (left) and the P-LIG (right). (b) EDS mapping images for the M-LIG devices. (c) XPS survey spectra of the M-LIG devices.

 doi:10.20944/preprints202401.0424.v1

2.3. Gas-sensing performance characterizations

With increasing temperature, our P-LIG sensor device shows a decrease in resistance (Figure S4); its responses toward 1000 ppm of NO2 were examined to determine the optimal operating temperature. The relative response, $\Delta R/R_0$ (%), of the sensor was calculated by equation (2):

$$\Delta R/R_0(\%) = \left(\frac{R_g - R_0}{R_0}\right) \times 100 \quad (2)$$

where R_g and R_0 are the sensor resistances under the analyte gas and under N_2, respectively. Figure S1 shows comparison graphs for the response of the P-LIG sensor device to 1000 ppm NO_2 as the temperature was varied from 50°C to 150°C. The response shows an approximately twofold increase as the temperature was increased from 50°C to 100°C; however, once the response reached its maximum at 100°C, it decreased as the temperature was increased further to 150°C, where its value was even lower than that at 50°C. Because adsorption and desorption are temperature-sensitive processes, the deterioration in response at 150°C might be attributable to a decrease of the Debye length as the charge-carrier density increases at high temperatures and also to the untimely desorption of the adsorbed gas molecules bound to the graphene before an electrical interaction occurred between them.[30–32] These factors might lead to a shift of the baseline resistance, thereby hindering the detection of a minute variation in resistance that occurs via gas adsorption or desorption. Therefore, the temperature of 100°C was selected as the optimal operating temperature for all of the gas-sensing tests.

After optimizing the operation temperature, we exposed the P-LIG sensor device to different gas concentrations ranging from 250 to 1500 ppm for both NO_2 and NH_3 to investigate the sensitivity of the LIG devices. The results in Figure S5 show that the response saturation started from 500 ppm of NO_2, whereas no substantial variation in response was observed for elevated NH_3 concentrations. Because the highest responses were detected for 1000 ppm NO_2 and also 1000 ppm NH_3, the gas concentration of 1000 ppm was chosen for NO_2/NH_3 response tests to evaluate the influence of metal dopants on the LIG gas-sensing performance.

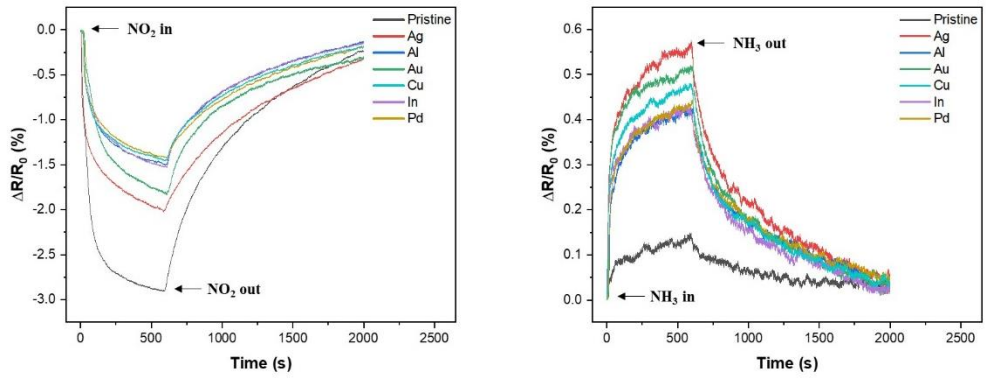

Figure 3. Comparison plots for the responses of the P- and M-LIG sensor devices toward (a) 1000 ppm of NO_2 and (b) 1000 ppm of NH_3.

Preprints.org (www.preprints.org) | NOT PEER-REVIEWED | Posted: 5 January 2024 doi:10.20944/preprints202401.0424.v1

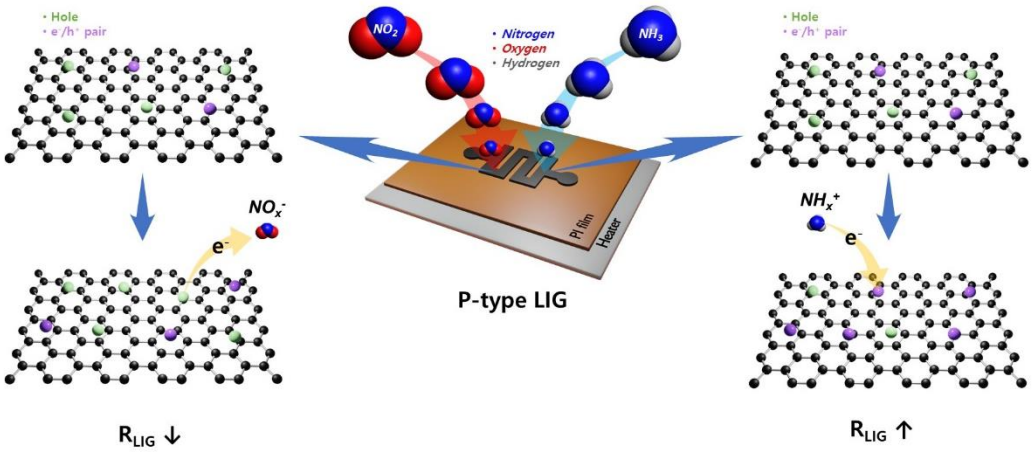

Figure 4. Schematics of the gas-sensing mechanisms of the P-LIG sensor device toward NO2 (left, oxidizing gas) and NH3 (right, reducing gas).

Figure 3 shows a set of seven single-response cycles for the P- and M-LIG sensor devices exposed to 1000 ppm NO_2 (a) and NH_3 (b) at 100°C while a DC bias of 1 V was applied. In fact, all of the tests were run with three on–off cycles and each cycle consisted of 10 min analyte-gas purging and 25 min N_2 purging for the "on" and "off" cycles, respectively (Figure S6 and S7). When the devices were exposed to NO_2, a negative trend in $\Delta R/R_0(\%)$ was observed for all of the devices as the resistance decreased, whereas a positive tendency was observed as the resistance increased upon exposure to NH_3. This typical phenomenon can be observed when the graphene with a p-type conducting characteristic is in contact with an oxidizing agent (i.e., electron acceptor, NO_2) or reducing agent (i.e., electron donor, NH_3).[10,33,34] In addition, graphene synthesized under ambient conditions typically exhibits p-type conduction, where the major carriers are holes, because of adsorbed oxygen or water molecules.[35] Thus, as depicted in Figure 4, once the p-type graphene is exposed to an oxidizing NO_2 gas, the hole accumulation within the graphene occurs after electron migration from graphene to the gas molecules, which results in a decrease in resistance. Meanwhile, upon contact of the sensors with a reducing NH_3 gas, electron injection from gas molecules into graphene reduces the major carrier concentration of the graphene; as a result, the overall resistance increases. In addition, we note that the sensitivity ($S, |\Delta R/R_0(\%)|$) of both the P- and M-LIG sensor devices toward NO_2 gas is much higher than that toward NH_3 gas. As the first-principles study validated, this difference might be attributable to the higher adsorption energy (~67 meV) and charge transfer (~0.099e from graphene to a gas molecule) of NO_2 compared with those of NH_3 (~31 meV and ~0.027e for the adsorption energy and charge transfer from molecules to graphene, respectively) when they are adsorbed onto the surface of graphene.[10,36]

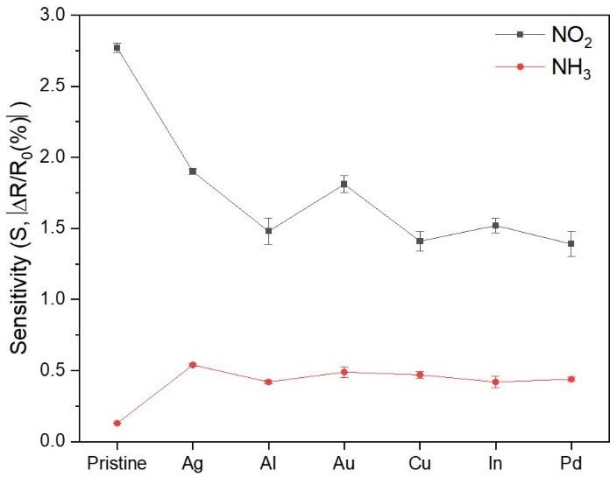

 doi:10.20944/preprints202401.0424.v1

Figure 5. Sensitivity comparison plot for the P- and M-LIG sensor devices upon exposure to NO_2 (black) and NH_3 (red).

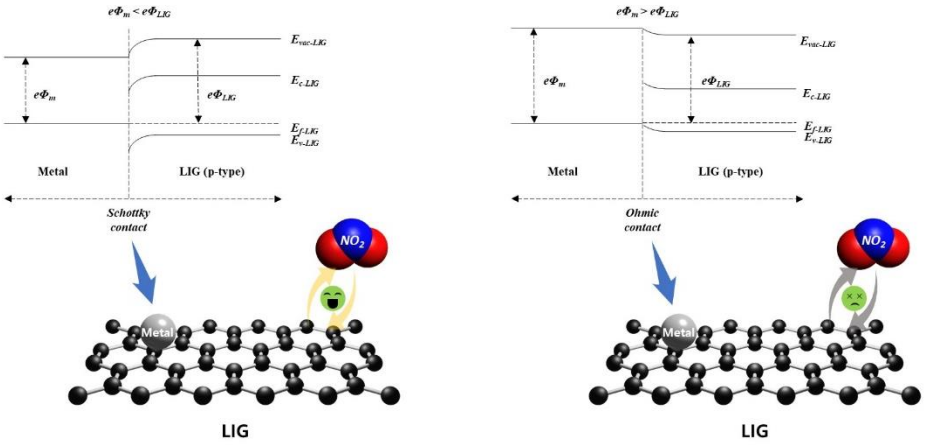

Figure 6. Schematics showing the formation of a Schottky contact ($\Phi_m < \Phi_{LIG}$, left) and an Ohmic contact ($\Phi_m > \Phi_{LIG}$, right) in the M-LIG sensor devices.

To investigate the role of metal incorporation into the LIG on the gas-sensing performance of LIG-based sensors, we selected metal dopants frequently used in first-principles studies of metal-doped graphene (i.e., Ag, Al, Au, Cu, In, and Pd) to fabricate the M-LIG sensor devices.[11–14,16,17,36–40] As shown in Figure 5, the NO_2 response of the P-LIG device was superior to those of all of the M-LIG devices. This deterioration in NO_2 response of the M-LIG sensor devices cannot be explained by a simple difference in work function between the metal NPs and LIG. (When work-function differences between pure metals and graphene are considered, the sensitivity should show a trend of high-work-function metal-doped LIG < LIG < low-work-function metal-doped LIG.) The deterioration is rather explained by considering the sophisticated interactions between the metal NPs and LIG, the metal NPs and NO_2, and the LIG and NO_2. To this end, an interpretation based on the electronic structures of metal NPs, LIG, and gaseous analytes can be applied to understand the inferior responses of the m-LIG sensor devices toward NO_2.

First, we focused on the oxidation of metals on the surface of LIG. According to the analyzed XPS data, the M-LIG sensor devices with highly oxidized surfaces (Al, Cu, and Pd) demonstrate weaker responses to NO_2 than the devices with metals with relatively weakly oxidized surfaces (Ag, Au, and In). In general, the oxidation of a metal dopant on a sensing layer can modify the surface properties and the overall electronic structure of the sensing material by changing the charge state.[41–43] Moreover, the oxidized metal dopant can react with a vacancy in the host material (p-type) at a relatively high temperature (~100°C) to generate electrons via the electronic compensation mechanism. These electrons can contribute to a reduction of the hole carrier concentration through electron–hole recombination, negatively affecting the sensing performance of the p-type LIG.[44–46] In addition, compared with the pure metallic catalysts on LIG, their undesirable oxidation might diminish the spill-over effect by shrinking its active reaction site for gas molecules and, consequently, decreasing the sensitivity[47,48] Among the highly oxidized metal-doped LIG devices, the NO_2 response is ranked in order of Al, Cu, and Pd and their work-function order is Pd > Cu > Al.[12] The slightly stronger response of the Al-doped LIG device might originate from the formation of a hole-depletion zone in the LIG adjacent to the interface with Al NPs.[49] Because the work function of Al is lower than that of multilayered graphene, a Schottky contact is generated by a large Fermi-level difference between the Al metal and p-type graphene, which leads to the formation of the hole-depletion zone in the LIG.[12,50] This hole depletion promotes electron charge transfer from the LIG to gas molecules (Figure 6) and thus enhances the sensing response to NO_2.[7] By contrast, the adsorption of the higher-work-function Cu onto LIG creates a hole accumulation zone at the interface

 doi:10.20944/preprints202401.0424.v1

via the p-doping effect on the LIG.[49] This hole accumulation zone impedes electron charge transfer from the LIG to NO_2 molecules, thereby weakening the response to NO_2.

Oddly, the surface of the Pd-doped LIG is highly oxidized even though Pd is a noble metal; consequently, the Pd-doped LIG device exhibits the weakest response among the investigated devices. The Pd-doped LIG device exhibiting the weakest response to NO_2 among the investigated devices, in addition to being attributable to the weak surface oxidation of Pd, In addition to its highly oxidized surface, the weakest response of the Pd-doped LIG deivce towards NO_2 might also be attributable to Pd substantially damaging the conical points of graphene at *K* via hybridization between the graphene p_z states and the Pd *d* states, impeding the charge transfer of graphene.[14] In the case of the relatively less-oxidized metals, the M-LIG devices show a response order of Ag, Au, and In toward NO_2. Although the work function of In is lower than that of Ag and Au, its corresponding response is inferior to the others and is even similar to that of highly oxidized metals.[13] Chandni et al.[39,40] and Jia et al. investigated the transport of In adatoms on graphene and found that In adatoms drastically reduce the carrier mobility of the graphene and increase the level of charge-density inhomogeneity in the graphene, possibly resulting in a weaker response toward NO_2. In a comparison of the Ag- and Au-doped LIG devices, the Ag-LIG device exhibits a slightly stronger response because of the lower work function of Ag.[12]

In contrast to the NO_2 response results, all of the investigated metals appear to have participated in the enhancement of the NH_3 gas response (Figure 3(b) and Figure 5). An approximately three- to four-fold increase in relative response was observed in the M-LIG sensor devices compared with the P-LIG device. As previously mentioned, NH_3 exhibits a lower adsorption energy and a lower charge transfer rate than NO_2; in this case, the chemical sensitization effect of metal NPs on LIG might play a dominant role in the sensing mechanism for NH_3 detection. In general, metal NPs on a sensing film tend to offer more active sensing sites for the analyte gas and to catalytically promote the dissociation of gas molecules into their more reactive status, leading to a sensitivity enhancement.[51–53] Similar to the influence of metal oxidation on the NO_2 response, greater metal oxidation led to a lower NH_3 response; notably, however, reducing the charge carrier mobility by introducing In as a dopant might profoundly lower the sensitivity, resulting in the weakest response toward NH_3. Meanwhile, among the M-LIG sensor devices, the Ag-doped LIG device exhibited the strongest response to NH_3 as its ranked order in response toward NO_2.

3. Conclusions

The LDW method, which is known as a facile and effective route for fabricating graphene, was used to produce LIG gas-sensor devices on flexible PI films, and their sensing performance toward an oxidizing agent (NO_2) and a reducing agent (NH_3) was investigated. For comparison, various metals such as Ag, Al, Au, Cu, In, and Pd were used to construct the M-LIG sensor devices; the influence of metal incorporation on the sensing response was also observed. The experimental results showed that our LIG has a certain degree of defects and multilayers and that doping metals into this graphene led to an enhanced response to NH_3 gas but a diminished response to NO_2 gas. This result is attributable to the metal NPs providing a large specific surface area for the LIG, enabling the detection of NH_3 gas molecules, which have a lower adsorption energy and less charge transfer than NO_2 molecules. On the contrary, the NO_2 gas sensing might be strongly affected by the alteration of the electronic structure of the M-LIGs via either the oxidation of metal dopants on the LIG surface or the formation of hole-depletion/accumulation areas at the interface as a result of the work-function difference between the metal dopant and the LIG. Given the lack of relevant practical research on the gas-sensing performance of metal-doped 3D-structured graphene with defects and multilayers like LIG, this work could not only lead to better understanding of its sensing mechanism through clarifying the interactions between the LIG and gas molecules, metal dopants and the LIG, and gas molecules and metal dopants but could also support first-principles studies of metal-doped graphene systems in gas detection, ultimately contributing to the development of high-performance LIG-based gas sensors.

 doi:10.20944/preprints202401.0424.v1

4. Materials and Methods

4.1. Synthesis of LIG on PI

The serpentine-patterned LIG (Figure 7) was fabricated directly onto a commercial PI film (125 μm thick, Kapton polyimide film, DuPont, USA) with a CO_2 laser system platform (VLS 2.30DT, power P_{max} = 30 W, speed S_{max} = 1270 mm·s^{-1}, wavelength λ = 10.6 μm, Universal Laser Systems, USA). Two-circle shapes of LIG were formed on each top and bottom edge to provide electrical connections. The optimized laser parameters were a laser power of 4 W, scanning speed of 127 mm·s^{-1}, and an image density of 500 pulses per inch (PPI, 1 inch = 25.4 mm); these parameters were used for fabricating all of the devices; the desired pattern was designed via AutoCAD and CorelDRAW.

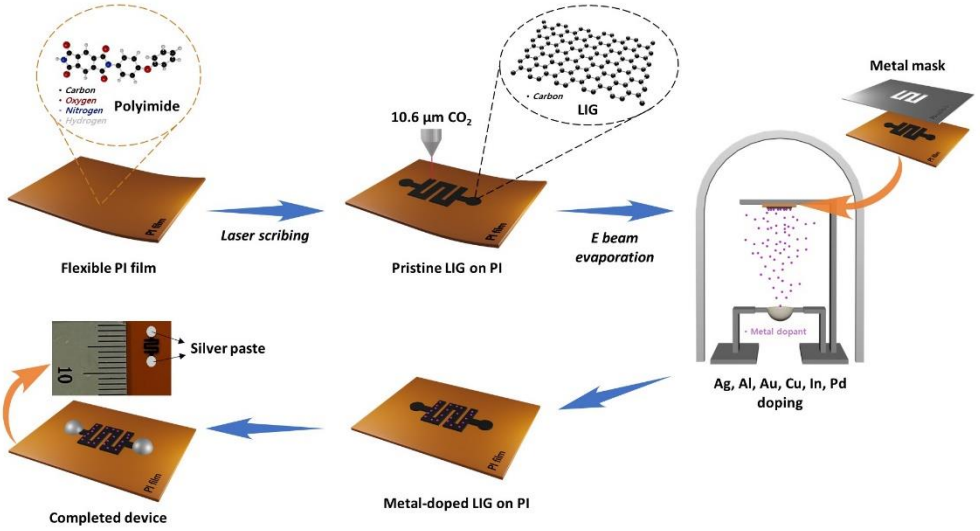

Figure 7. Schematics of the fabrication of P-LIG and M-LIG sensor devices.

4.2. Preparation of P-LIG and M-LIG Devices

As shown in Figure 7, metal NPs (Ag, Al, Au, Cu, In, and Pd) were deposited onto the pre-fabricated P-LIG device with metal (SUS304) stencil masks using a thermal evaporator system. For each metal deposition process, a separate mask was used to avoid cross-contamination; in addition, metals were deposited to a thickness of 4 nm, which was measured using a quartz crystal monitor (QCM), at a deposition rate of ~0.2 Å·s^{-1} under a pressure of ~1×10^{-7} torr. After the deposition, the top/bottom circle areas were coated with Ag paste for all of the devices to allow connection to the external electronics.

4.3. Bare LIG and Metal-doped LIG Characterizations

The 3D porous structure of the LIG was characterized by scanning electron microscopy (SEM, Philips XL30S, FEI, The Netherlands). Energy-dispersive X-ray spectroscopy (EDS, Bruker Quantax 200, USA) was performed with an XFlash 6 Si-drift detector to observe dispersed metal NPs on the LIG). X-ray photoelectron spectroscopy (XPS) and Raman spectroscopy were carried out using a photoelectron spectrometer (AXIS Supra+, Kratos Analytical, UK) and a laser (1064 nm Nd:YAG) Raman spectrometer (Bruker FRA 106/S, USA), respectively

4.4. Sensor Testing Equipment

A custom-designed testing chamber with a volume of 100 mL and a homemade probe station with a ceramic heater were constructed to conduct the gas-sensing test. Both the gas concentration and the flow rate of the gas analytes were precisely regulated by mass flow controllers (MFCs)

 doi:10.20944/preprints202401.0424.v1

connected to the inlet of the chamber. At a constant flow rate of 1 L·min^{-1}, every test was run with three on/off cycles, where an individual cycle consisted of 10 min of purging with the gas/N_2 mixture followed by 25 min of purging with pure N_2. Two probes of the probe station were attached to the Ag-pasted areas of the sensor device and were used to measure the current (I) and voltage (V) while a constant DC voltage (1 V) was applied to the device. The real-time change in the electrical resistance of the device was monitored and recorded using a source meter (Keithley 2612B, Keithley Instruments, USA). The temperature of the ceramic heater equipped in the probe station was controlled by an electronic heating system, and the operation temperature was optimized at 100°C (Figure S1) for all of the tests.

Supplementary Materials: The following supporting information can be downloaded at: Preprints.org

Author Contributions: Formal analysis, investigation, visualization and writing-original draft preparation, D.Kwak.; resources, H.Kim. and B.G.Kim.; software, S.H.Jang. and H.Chang.; writing-review and editing, D.Cho. and J.O.Lee.; supervision and validation, B.G.Kim., H.Chang. and J.O.Lee.; conceptualization and project administration, H.Chang. and J.O.Lee.; funding acquisition, H.Chang. and J.O.Lee. All authors have read and agreed to the published version of the manuscript.

Funding: This research is funded by KNPA, MSIT, MOTIE, ME, and NFA (NRF-2017M3D9A1073861) and by the Korea Research Institute of Chemical Technology (SI2251-10).

Data Availability Statement: We encourage all authors of articles published in MDPI journals to share their research data. In this section, please provide details regarding where data supporting reported results can be found, including links to publicly archived datasets analyzed or generated during the study. Where no new data were created, or where data is unavailable due to privacy or ethical restrictions, a statement is still required. Suggested Data Availability Statements are available in section "MDPI Research Data Policies" at https://www.mdpi.com/ethics.

Acknowledgments: This research was supported by the Multi-Ministry Collaborative R&D Program (Development of Techniques for Identification and Analysis of Gas Molecules to Protect Against Toxic Substances) through the NRF funded by KNPA, MSIT, MOTIE, ME, and NFA (NRF-2017M3D9A1073861) and by the Korea Research Institute of Chemical Technology (SI2251-10)

Conflicts of Interest: The authors declare no conflicts of interest.

References

1. Peng, Z.; Tao, L.-Q.; Zou, S.; Zhu, C.; Wang, G.; Sun, H.; Ren, T.-L. A Multi-functional NO2 gas monitor and Self-Alarm based on Laser-Induced graphene. *Chemical Engineering Journal* **2022**, *428*, doi:10.1016/j.cej.2021.131079.
2. Yan, W.; Yan, W.; Chen, T.; Xu, J.; Tian, Q.; Ho, D. Size-Tunable Flowerlike MoS2 Nanospheres Combined with Laser-Induced Graphene Electrodes for NO2 Sensing. *ACS Applied Nano Materials* **2020**, *3*, 2545-2553, doi:10.1021/acsanm.9b02614.
3. Kwon, B.; Bae, H.; Lee, H.; Kim, S.; Hwang, J.; Lim, H.; Lee, J.H.; Cho, K.; Ye, J.; Lee, S.; et al. Ultrasensitive N-Channel Graphene Gas Sensors by Nondestructive Molecular Doping. *ACS Nano* **2022**, *16*, 2176-2187, doi:10.1021/acsnano.1c08186.
4. Singh, A.; Shiby, S.; Sahu, A.; Pachori, P.; Tanwar, M.; Kumar, R.; Palani, A.I. Parametric investigation on laser interaction with polyimide for graphene synthesis towards flexible devices. *Journal of Physics D: Applied Physics* **2022**, *56*.
5. Yuan, W.; Shi, G. Graphene-based gas sensors. *Journal of Materials Chemistry A* **2013**, *1*, 10078-10091.
6. Eriksson, J.; Puglisi, D.; Kang, Y.H.; Yakimova, R.; Spetz, A.L. Adjusting the electronic properties and gas reactivity of epitaxial graphene by thin surface metallization. *Physica B: Condensed Matter* **2014**, *439*, 105-108.
7. Cho, B.; Yoon, J.; Hahm, M.G.; Kim, D.-H.; Kim, A.R.; Kahng, Y.H.; Park, S.-W.; Lee, Y.-J.; Park, S.-G.; Kwon, J.-D. Graphene-based gas sensor: metal decoration effect and application to a flexible device. *Journal of Materials Chemistry C* **2014**, *2*, 5280-5285.
8. Javey, A.; Guo, J.; Wang, Q.; Lundstrom, M.; Dai, H. Ballistic carbon nanotube field-effect transistors. *nature* **2003**, *424*, 654-657.
9. Chen, Z.; Appenzeller, J.; Knoch, J.; Lin, Y.-m.; Avouris, P. The role of metal− nanotube contact in the performance of carbon nanotube field-effect transistors. *Nano letters* **2005**, *5*, 1497-1502.

10. Leenaerts, O.; Partoens, B.; Peeters, F. Adsorption of H 2 O, N H 3, CO, N O 2, and NO on graphene: A first-principles study. *Physical Review B* **2008**, *77*, 125416.
11. Singhal, A.V.; Charaya, H.; Lahiri, I. Noble metal decorated graphene-based gas sensors and their fabrication: a review. *Critical Reviews in Solid State and Materials Sciences* **2017**, *42*, 499-526.
12. Giovannetti, G.; Khomyakov, P.A.; Brocks, G.; Karpan, V.v.; van den Brink, J.; Kelly, P.J. Doping graphene with metal contacts. *Physical review letters* **2008**, *101*, 026803.
13. Chan, K.T.; Neaton, J.; Cohen, M.L. First-principles study of metal adatom adsorption on graphene. *Physical Review B* **2008**, *77*, 235430.
14. Khomyakov, P.; Giovannetti, G.; Rusu, P.; Brocks, G.v.; Van den Brink, J.; Kelly, P.J. First-principles study of the interaction and charge transfer between graphene and metals. *Physical Review B* **2009**, *79*, 195425.
15. Liang, X.-Y.; Ding, N.; Ng, S.-P.; Wu, C.-M.L. Adsorption of gas molecules on Ga-doped graphene and effect of applied electric field: A DFT study. *Applied Surface Science* **2017**, *411*, 11-17.
16. Ni, J.; Quintana, M.; Song, S. Adsorption of small gas molecules on transition metal (Fe, Ni and Co, Cu) doped graphene: A systematic DFT study. *Physica E: Low-dimensional Systems and Nanostructures* **2020**, *116*, 113768.
17. Yang, L.; Xiao, W.; Wang, J.; Li, X.; Wang, L. Formaldehyde gas sensing properties of transition metal-doped graphene: a first-principles study. *Journal of Materials Science* **2021**, *56*, 12256-12269.
18. Zhao, M.; Dong, F.; Yan, L.; Xu, L.; Zhang, X.; Chen, P.; Song, Z.; Chu, W. High efficiency room temperature detection of NO 2 gas based on ultrathin metal/graphene devices. *RSC advances* **2016**, *6*, 84082-84089.
19. Zhu, J.; Cho, M.; Li, Y.; Cho, I.; Suh, J.-H.; Del Orbe, D.; Jeong, Y.; Ren, T.-L.; Park, I. Biomimetic Turbinate-like Artificial Nose for Hydrogen Detection Based on 3D Porous Laser-Induced Graphene. *ACS Applied Materials & Interfaces* **2019**, *11*, 24386-24394.
20. Tseng, S.-F.; Chen, P.-S.; Hsu, S.-H.; Hsiao, W.-T.; Peng, W.-J. Investigation of fiber laser-induced porous graphene electrodes in controlled atmospheres for ZnO nanorod-based NO2 gas sensors. *Applied Surface Science* **2023**, *620*, doi:10.1016/j.apsusc.2023.156847.
21. Wang, F.; Wang, K.; Zheng, B.; Dong, X.; Mei, X.; Lv, J.; Duan, W.; Wang, W. Laser-induced graphene: preparation, functionalization and applications. *Materials technology* **2018**, *33*, 340-356.
22. Stanford, M.G.; Yang, K.; Chyan, Y.; Kittrell, C.; Tour, J.M. Laser-Induced Graphene for Flexible and Embeddable Gas Sensors. *ACS Nano* **2019**, *13*, 3474-3482, doi:10.1021/acsnano.8b09622.
23. Dosi, M.; Lau, I.; Zhuang, Y.; Simakov, D.S.A.; Fowler, M.W.; Pope, M.A. Ultrasensitive Electrochemical Methane Sensors Based on Solid Polymer Electrolyte-Infused Laser-Induced Graphene. *ACS Appl Mater Interfaces* **2019**, *11*, 6166-6173, doi:10.1021/acsami.8b22310.
24. Ye, R.; James, D.K.; Tour, J.M. Laser-Induced Graphene: From Discovery to Translation. *Adv Mater* **2019**, *31*, e1803621, doi:10.1002/adma.201803621.
25. Wang, Y.-n.; Gan, J.; Wang, D.-m.; Xin, H.-h.; Zhu, Y.-f. Characteristics and electrical properties of polyimide films fluorinated for different durations. *Materials Today Communications* **2021**, *26*, 102098.
26. Robertson, A.C.F.a.J. Interpretation of Raman spectra of disordered and amorphous carbon. *Physical review B* **2000**, *61*, 14095.
27. Ferrari, A.C.; Robertson, J. Interpretation of Raman spectra of disordered and amorphous carbon. *Physical review B* **2000**, *61*, 14095.
28. Yao, J.; Liu, L.; Zhang, S.; Wu, L.; Tang, J.; Qiu, Y.; Huang, S.; Wu, H.; Fan, L. Metal-incorporated laser-induced graphene for high performance supercapacitors. *Electrochimica Acta* **2023**, *441*, 141719.
29. Zhang, Y.; Franklin, N.W.; Chen, R.J.; Dai, H. Metal coating on suspended carbon nanotubes and its implication to metal–tube interaction. *Chemical Physics Letters* **2000**, *331*, 35-41.
30. Kim, T.; Eom, T.H.; Jang, H.W. Self-activated Graphene Gas Sensors: A Mini Review. *Journal of Sensor Science and Technology* **2020**, *29*, 220-226.
31. Eranna, G.; Joshi, B.; Runthala, D.; Gupta, R. Oxide materials for development of integrated gas sensors—a comprehensive review. *Critical Reviews in Solid State and Materials Sciences* **2004**, *29*, 111-188.
32. Kim, T.Y.; Park, C.H.; Marzari, N. The Electronic Thermal Conductivity of Graphene. *Nano Lett* **2016**, *16*, 2439-2443, doi:10.1021/acs.nanolett.5b05288.
33. Huang, B.L., Z.;Liu, Z.; Zhou, G.; Hao, S.; Wu, J.; Gu, B-L.; Duan, W. . Adsorption of gas molecules on graphene nanoribbons and its implication for nanoscale molecule sensor. *The Journal of Physcial Chemistry C* **2008**, *112*, 13442-13446.

34. Varghese, S.S.; Lonkar, S.; Singh, K.K.; Swaminathan, S.; Abdala, A. Recent advances in graphene based gas sensors. *Sensors and Actuators B: Chemical* **2015**, *218*, 160-183, doi:10.1016/j.snb.2015.04.062.
35. Jung, I.; Dikin, D.A.; Piner, R.D.; Ruoff, R.S. Tunable electrical conductivity of individual graphene oxide sheets reduced at "low" temperatures. *Nano letters* **2008**, *8*, 4283-4287.
36. Zhou, M.; Lu, Y.-H.; Cai, Y.-Q.; Zhang, C.; Feng, Y.-P. Adsorption of gas molecules on transition metal embedded graphene: a search for high-performance graphene-based catalysts and gas sensors. *Nanotechnology* **2011**, *22*, 385502.
37. Rad, A.S.; Foukolaei, V.P. Density functional study of Al-doped graphene nanostructure towards adsorption of CO, CO2 and H2O. *Synthetic Metals* **2015**, *210*, 171-178.
38. Subrahmanyam, K.; Manna, A.K.; Pati, S.K.; Rao, C. A study of graphene decorated with metal nanoparticles. *Chemical Physics Letters* **2010**, *497*, 70-75.
39. Jia, Z.; Yan, B.; Niu, J.; Han, Q.; Zhu, R.; Yu, D.; Wu, X. Transport study of graphene adsorbed with indium adatoms. *Physical Review B* **2015**, *91*, 085411.
40. Chandni, U.; Henriksen, E.A.; Eisenstein, J. Transport in indium-decorated graphene. *Physical Review B* **2015**, *91*, 245402.
41. Mirzaei, A.; Bharath, S.P.; Kim, J.-Y.; Pawar, K.K.; Kim, H.W.; Kim, S.S. N-Doped Graphene and Its Derivatives as Resistive Gas Sensors: An Overview. *Chemosensors* **2023**, *11*, 334.
42. Chakraborty, N.; Mondal, S. Dopant-mediated surface charge imbalance for enhancing the performance of metal oxide chemiresistive gas sensors. *Journal of Materials Chemistry C* **2022**, *10*, 1968-1976.
43. Kropp, T.; Mavrikakis, M. Transition metal atoms embedded in graphene: how nitrogen doping increases CO oxidation activity. *ACS Catalysis* **2019**, *9*, 6864-6868.
44. Wang, S.; Huang, D.; Xu, S.; Jiang, W.; Wang, T.; Hu, J.; Hu, N.; Su, Y.; Zhang, Y.; Yang, Z. Two-dimensional NiO nanosheets with enhanced room temperature NO 2 sensing performance via Al doping. *Physical Chemistry Chemical Physics* **2017**, *19*, 19043-19049.
45. Wang, C.; Cui, X.; Liu, J.; Zhou, X.; Cheng, X.; Sun, P.; Hu, X.; Li, X.; Zheng, J.; Lu, G. Design of superior ethanol gas sensor based on Al-doped NiO nanorod-flowers. *Acs Sensors* **2016**, *1*, 131-136.
46. Moafi, A.; Heidari, O.; Soltannia, B.; Wlodarski, W.; Shahi, F.; Parvin, P. Reduction of metal nanoparticle decorated flexible graphene oxide by laser at various temperatures and under selected atmospheres. *Carbon Trends* **2022**, *6*, 100140.
47. Eom, W.; Jang, J.-S.; Lee, S.H.; Lee, E.; Jeong, W.; Kim, I.-D.; Choi, S.-J.; Han, T.H. Effect of metal/metal oxide catalysts on graphene fiber for improved NO2 sensing. *Sensors and Actuators B: Chemical* **2021**, *344*, 130231.
48. Karim, W.; Spreafico, C.; Kleibert, A.; Gobrecht, J.; VandeVondele, J.; Ekinci, Y.; van Bokhoven, J.A. Catalyst support effects on hydrogen spillover. *Nature* **2017**, *541*, 68-71.
49. Kim, B.-K.; Park, N.; Na, P.S.; So, H.-M.; Kim, J.-J.; Kim, H.; Kong, K.-J.; Chang, H.; Ryu, B.-H.; Choi, Y. The effect of metal cluster coatings on carbon nanotubes. *Nanotechnology* **2005**, *17*, 496.
50. Rut'kov, E.V.; Afanas'eva, E.Y.; Gall, N.R. Graphene and graphite work function depending on layer number on Re. *Diamond and Related Materials* **2020**, *101*, doi:10.1016/j.diamond.2019.107576.
51. Franke, M.E.; Koplin, T.J.; Simon, U. Metal and metal oxide nanoparticles in chemiresistors: does the nanoscale matter? *small* **2006**, *2*, 36-50.
52. Yamazoe, N. New approaches for improving semiconductor gas sensors. *Sensors and actuators B: Chemical* **1991**, *5*, 7-19.
53. Kohl, D. The role of noble metals in the chemistry of solid-state gas sensors. *Sensors and Actuators B: Chemical* **1990**, *1*, 158-165.